

# CRPropa: A Numerical Tool for the Propagation of UHE Cosmic Rays, $\gamma$ -rays and Neutrinos

Eric Armengaud<sup>a,b,c</sup>, Günter Sigl<sup>a,b</sup>, Tristan Beau<sup>a</sup>, Francesco Miniati<sup>d</sup>

<sup>a</sup> *APC, Bâtiment Condorcet, 10 rue Alice Domon et Léonie Duquet, 75205 Paris Cedex 13, France - UMR 7164 (CNRS, Université Paris Diderot Paris 7, CEA, Observatoire de Paris)*

<sup>b</sup> *GReCO, Institut d'Astrophysique de Paris, C.N.R.S., 98 bis boulevard Arago, F-75014 Paris, France*

<sup>c</sup> *CEA, DSM, DAPNIA, Centre d'Etudes de Saclay, F-91191 Gif-sur-Yvette Cedex, France*

<sup>d</sup> *Physics Department, ETH Zürich, 8093 Zürich, Switzerland*

---

## Abstract

To understand the origin of ultra-high energy cosmic rays (UHECRs, defined to be above  $10^{18}$  eV), it is required to model in a realistic way their propagation in the Universe. UHECRs can interact with low energy radio, microwave, infrared and optical photons to produce electron/positron pairs or pions. The latter decay and give rise to neutrinos and electromagnetic cascades extending down to MeV energies. In addition, deflections in cosmic magnetic fields can influence the spectrum and sky distribution of primary cosmic rays and, due to the increased propagation path length, the secondary neutrino and  $\gamma$ -ray fluxes. Neutrino,  $\gamma$ -ray, cosmic ray physics and extra-galactic magnetic fields are, therefore, strongly linked subjects and should be considered together in order to extract maximal information from existing and future data, like the one expected from the Auger Observatory. For that purpose, we have developed CRPropa, a publicly-available numerical package which takes into account interactions and deflections of primary UHECRs as well as propagation of secondary electromagnetic cascades and neutrinos. CRPropa allows to compute the observable properties of UHECRs and their secondaries in a variety of models for the sources and propagation of these particles. Here we present physical processes taken into account as well as benchmark examples; a detailed documentation of the code can be found on our web site.

---

## 1 Introduction

Astroparticle physics is currently experimentally driven and involves many different existing or planned projects ranging from UHECR observatories such as the Pierre Auger Observatory [1], to neutrino telescopes [2], as well as ground and space based  $\gamma$ -ray detectors operating at TeV and GeV energies, respectively [3]. It is clear that GeV-TeV  $\gamma$ -ray and neutrino astronomy will prove an invaluable tool to unveil the sources, and probe into the mechanism, of UHECRs. Even if a putative source were to produce exclusively UHECRs, photo-pion [4] and pair production by protons on the cosmic microwave background (CMB) would lead to guaranteed secondary photon and neutrino fluxes that could be detectable. Furthermore, spectra, power and sky distributions of both primary UHECRs and secondary  $\gamma$ -rays and neutrinos depend on the poorly known large scale cosmic magnetic fields.

It is, therefore, desirable to have a numerical tool that can treat the interface between UHECR,  $\gamma$ -ray and neutrino astrophysics, and large scale magnetic fields. To this end, we have recently merged our Monte Carlo code for simulating three dimensional propagation of UHECRs in a structured, magnetized Universe [5] with a one-dimensional transport code that solves electromagnetic (EM) cascades and neutrino propagation [6]. We discuss the limitations due to the one-dimensional approximation and implement a procedure to test the resulting uncertainty on the EM cascade on the observable fluxes. With the present paper, we release a public version of this code which we hope will be useful for the cosmic ray,  $\gamma$ -ray and neutrino communities.

In the following, we present the relevant interactions and propagation phenomena taken into account, and the propagation algorithms applied in CRPropa. We also present a few examples of how to use the code in practice. The numerical package and its detailed documentation are available for downloading on the CRPropa website, <http://apcauger.in2p3.fr/CRPropa>.

We use natural units,  $c = \hbar = 1$  throughout this paper.

## 2 Propagation algorithms

UHECRs are injected at specified sources, and propagated step-by-step in either a one- or a three-dimensional environment. The trajectories are regularly sampled, or recorded only at specific locations (e.g. at a given distance from a source, or at an “observer” point). Each propagation step consists of integrating the Lorentz equations, and computing the interactions and possibly the secondaries generated by those interactions.

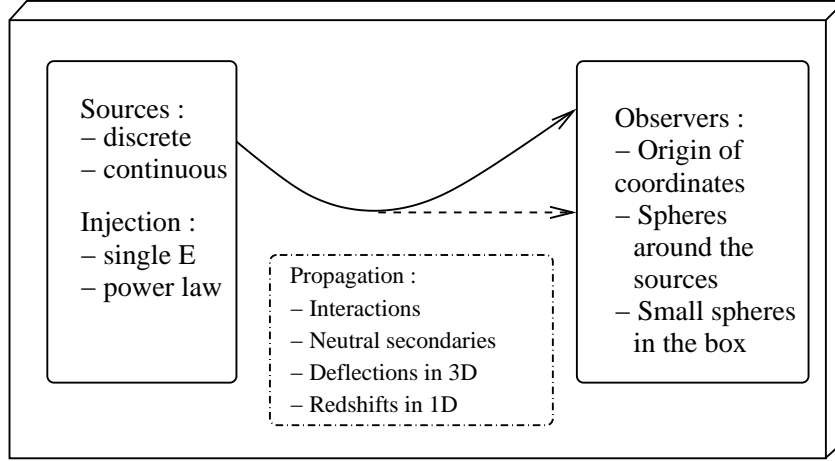


Fig. 1. Principle of the propagation algorithm. This scheme applies to all configurations.

In the 3-dimensionnal case, a “simulation box” is defined and periodic boundary conditions are assumed.

When deflections are taken into account, cosmological redshifts cannot be computed, because the propagation time until the particle reaches the observer is not known before hand. Therefore, redshift evolution is only accounted for in the 1D version of the package. The concordance cosmology is used for which, assuming a flat Universe, the Hubble rate  $H(z)$  at redshift  $z$  in the matter dominated regime,  $z \lesssim 10^3$ , is given by

$$H(z) = H_0 \left[ \Omega_m (1+z)^3 + \Omega_\Lambda \right]^{1/2}. \quad (1)$$

The parameters  $\Omega_m$  and  $\Omega_\Lambda$  can be freely chosen, their standard values being  $\Omega_m = 0.3$ ,  $\Omega_\Lambda = 0.7$ , and  $H_0 = h_0 100 \text{ km s}^{-1} \text{ Mpc}^{-1}$  with  $h_0 = 0.72$ .

The general principle of the simulations is shown in Fig. 1.

## 2.1 Nucleon Interactions

The most famous interaction of nucleons with the low-energy photon backgrounds is pion production, which generates the GZK feature. In order to handle pion production, we use the event generator SOPHIA [7], that has been explicitly designed to study this phenomenon and that uses the particle production cross-sections measured in accelerators. We have also augmented the SOPHIA package for interactions with a low energy extragalactic background light (EBL) with a general energy distribution. SOPHIA allows to determine the distribution of the stables particles generated by an interaction with a low-energy photon.

Pair production by protons (PPP) on the CMB, also known as Bethe-Heitler process, is taken into account as a continuous energy loss whose rate we evaluate following the expressions in Refs. [8,9]. For the spectrum of the pairs we exploit the fact that Bethe-Heitler and triplet pair production,  $e\gamma_b \rightarrow ee^+e^-$ , are analogous electromagnetic processes, their cross sections and inelasticities converging for relativistic pairs. Fig. 2 of Ref. [10] then shows that the spectrum of electron-positron pairs (heretofore simply referred to as electrons) generated by a proton of energy  $E$  can be approximated by a power-law energy distribution  $dn/dE_e \propto E_e^{-7/4}$ . Kinematics implies that this power law holds for  $E_{\min} \leq E_e \leq E_{\text{PPP}}$ , where the minimal and maximal energies are given by [6]

$$E_{\text{PPP}} \simeq \frac{4E^2\varepsilon}{4E\varepsilon + m_p^2} \simeq \frac{4.5 \times 10^{15} \left(\frac{E}{\text{EeV}}\right)^2 \left(\frac{\varepsilon}{\text{meV}}\right) \text{ eV}}{4.6 \times 10^{-3} \left(\frac{E}{\text{EeV}}\right) \left(\frac{\varepsilon}{\text{meV}}\right) + 1}$$

$$E_{\min} \simeq \frac{m_e^2}{8\varepsilon} \simeq 3.3 \times 10^{13} \left(\frac{\varepsilon}{\text{meV}}\right)^{-1} \text{ eV}. \quad (2)$$

In Eq. (2),  $m_p$  and  $m_e$  are the proton and electron masses, respectively,  $\varepsilon$  is the low energy target photon energy, and the approximation for  $E_{\min}$  holds for  $m_em_p \lesssim 4E\varepsilon \lesssim m_p^2$ . The average electron energy is then  $\overline{E_e} = \int_{E_{\min}}^{E_{\text{PPP}}} dE_e E_e E_e^{-7/4} / \int_{E_{\min}}^{E_{\text{PPP}}} dE_e E_e^{-7/4} \simeq 3 E_{\min}^{3/4} E_{\text{PPP}}^{1/4}$  which is indeed much smaller than the primary proton energy  $E$ . From Eq. (2), the inelasticity  $K \equiv \overline{E_e}/E$ , whose precise energy dependence can be found in Ref. [9], for  $m_em_p \lesssim 4E\varepsilon \lesssim m_p^2$  can thus be approximated by

$$K(E\varepsilon) \sim \frac{3}{2^{7/4}} \frac{m_e^{3/2}}{(E\varepsilon m_p)^{1/2}} \quad (3)$$

$$\simeq 3.4 \times 10^{-4} \left(\frac{E}{\text{EeV}}\right)^{-1/2} \left(\frac{\varepsilon}{\text{meV}}\right)^{-1/2},$$

This is consistent with Figs. 1 and 2 in Ref. [11]. For our purposes, we are not sensitive to the lower kinematic limit since the total energy produced  $\propto \int_{E_{\min}}^{E_{\text{PPP}}} dE_e E_e E_e^{-7/4} \simeq 4E_{\text{PPP}}^{1/4}$  is insensitive to  $E_{\min}$  as long as  $E_{\min} \ll E_{\text{PPP}}$ , but rather is dominated by the highest energies. As a consequence, the total proton energy loss rate due to pair production is dominated by the highest energy electrons close to  $E_{\text{PPP}}$ . However, because the production cross section of these highest energy electrons is much smaller than the one for the more numerous lower energy electrons, the average inelasticity Eq. (3) is nevertheless small, below  $10^{-3}$  everywhere above the pair production threshold. The spectrum and maximal energy of the pairs will be important for the synchrotron spectrum emitted by these electrons in an EGMF of strength  $B$  which peaks at  $\simeq 6.8 \times 10^{11} (E_e/10^{19} \text{ eV})^2 (B/0.1 \mu\text{G}) \text{ eV}$ .

Nucleons can be followed down to  $10^{17}$  eV with CRPropa, below which interactions become negligible.

## 2.2 Secondary Electromagnetic Cascades and Neutrinos

The secondary neutrinos from pion production of nucleons are propagated in straight lines assuming no energy losses except redshift effects.

All the EM products of these interactions are evolved using an EM cascade code based on Ref. [6]. The photons and pairs are followed until either their energy drops below 100 MeV or they reach an observer. All relevant interactions with a background photon  $\gamma_b$  are taken into account, namely single pair production (PP),  $\gamma\gamma_b \rightarrow e^+e^-$ , double pair production (DPP),  $\gamma\gamma_b \rightarrow e^+e^-e^+e^-$ , inverse Compton scattering (ICS),  $e\gamma_b \rightarrow e\gamma$ , and triplet pair production (TPP),  $e\gamma_b \rightarrow ee^+e^-$  (see also Ref. [12] for a detailed discussion of implemented interactions). In addition, synchrotron losses of electrons in the (in general) inhomogeneous EGMF are taken into account and the resulting lower energy synchrotron photons are also followed in the subsequent EM cascade.

This module has been applied to EM cascades from discrete magnetized proton sources in galaxy clusters in Ref. [13]. The EM cascades that are followed with the current version of CRPropa are propagated in straight lines, even in the case of 3-dimensionnal simulations for UHECRs: Every time a primary hadron interacts and initiates an EM cascade, it is assumed that the secondaries propagate along straight lines and it is checked whether the line of sight crosses the observer. If this is the case, the EM cascade module is called with the corresponding propagation distance and the projected magnetic field profile. Electrons in the EM cascade can of course be deflected in the EGMF, and we discuss here the validity of this one-dimensionnal approximation.

In a magnetic field of strength  $B$  the synchrotron cooling time for an electron of energy  $E_e$  is given by

$$t_{\text{synch}} = \frac{E_e}{dE_e/dt} = \frac{6\pi m_e^2}{\sigma_T E_e B^2} \quad (4)$$

$$\simeq 3.84 \text{ kpc} \left( \frac{E_e}{10^{15} \text{ eV}} \right)^{-1} \left( \frac{B}{\mu\text{G}} \right)^{-2},$$

where  $\sigma_T = 8\pi\alpha^2/3m_e^2$  is the Thomson cross section, with  $\alpha$  the fine structure constant. At high energies, in the Klein-Nishina regime the inverse Compton

energy loss length is roughly [12]

$$t_{\text{IC}} \lesssim 400 \text{ pc} \left( \frac{E_e}{10^{15} \text{ eV}} \right) \quad \text{for } E_e \gtrsim 10^{15} \text{ eV}. \quad (5)$$

At energies  $E_e \gtrsim 10^{18} \text{ eV}$  in Eq. (5) the energy loss length is between a factor  $\sim 30$  and a few hundred smaller than the numerical value in Eq. (5) due to contributions from the universal radio background. For a conservatively large  $t_{\text{IC}}$  at these energies we use an interpolation of Fig. 12 in [12] for the conservatively low radio background estimate. For  $E_e \lesssim 10^{15} \text{ eV}$ , ICS on the CMB is in the Thomson regime, with an interaction length  $\lambda_{\text{IC}} \sim 1/\sigma_T n_{\text{CMB}} \sim 1.2 \text{ kpc}$ , with  $n_{\text{CMB}}$  the CMB photon density. The energy lost by an electron at each interaction is  $\delta E_e \sim 4\epsilon E_e^2/3m_e^2$ , where  $\epsilon$  is a typical CMB photon energy. As a consequence, the energy loss length at energies below  $\sim 10^{15} \text{ eV}$  is:

$$t_{\text{IC}} \simeq \frac{3\lambda_{\text{IC}} m_e^2}{4\epsilon E_e} \sim 400 \text{ pc} \left( \frac{10^{15} \text{ eV}}{E_e} \right). \quad (6)$$

These length scales as well as the maximal propagation distance must be compared with the Larmor radius

$$r_L = \frac{E_e}{eB} \simeq 1.08 \text{ pc} \left( \frac{E_e}{10^{15} \text{ eV}} \right) \left( \frac{B}{\mu\text{G}} \right)^{-1}. \quad (7)$$

In order for a one-dimensional treatment of EM cascades to be a good approximation, the Larmor radius has to be much larger than either the total propagation length, the IC or the synchrotron loss lengths. For a given magnetic field, the condition  $r_L > A \times \min(t_{\text{synch}}, t_{\text{IC}})$  results in a condition  $E_e > E_c(B, A)$ , corresponding to deflections of the pairs by  $\lesssim (10/A) \times 6^\circ$ . This estimate of the deflection angle is however conservatively large: in realistic situations, magnetic fields are inhomogeneous with many reversals along the line of sight, and the actual deflection angle will be smaller provided the magnetic field coherence length is smaller than the energy loss length. The dependence of the “critical” energy  $E_c$  on  $B$  and  $A$  is shown in Fig. 2: For  $A = 10$ , corresponding to deflection by less than  $\sim 6^\circ$ ,  $E_c$  is determined by the competition between deflections and ICS for  $B \lesssim 300 \text{ pG}$ , or between deflection and synchrotron emission for  $B \gtrsim 300 \text{ pG}$ . For  $A = 100$ , corresponding to deflection by less than  $\sim 0.6^\circ$ , the transition between ICS and synchrotron emission as dominant losses to be compared with deflection occurs at  $B \simeq 20 \text{ pG}$ .

It turns out that whenever  $E_c(B, A) \lesssim 10^{15} \text{ eV}$ , the  $\gamma$ -ray flux from deflected pairs is sub-dominant. This is simply due to the fact that the pair flux at energies  $E_e \lesssim 10^{15} \text{ eV}$  is suppressed compared to the  $\gamma$ -ray flux which has a much larger interaction length and piles up below the pair production threshold. The  $\gamma$ -ray flux from deflected pairs can only be important if  $E_c(B, A) \gg 10^{15} \text{ eV}$

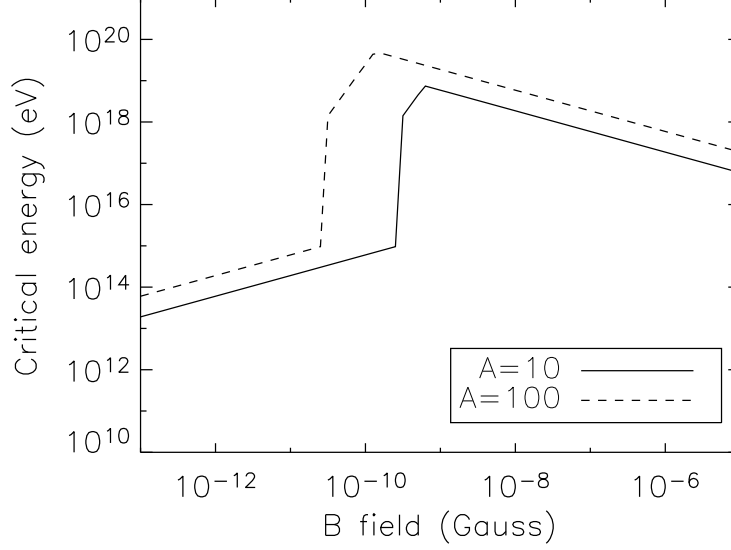


Fig. 2. The critical energy  $E_c$ , below which the  $e^{+/-}$  are deflected before cascading to lower energies, as a function of the order of magnitude of the magnetic field.  $E_c$  is obtained with the parameterization of various timescales given in the text, for  $A = 10$  (solid line) and  $A = 100$  (dashed line). This corresponds to cutting all pairs being deflected by more than  $\sim 6^\circ$  or  $0.6^\circ$ , respectively. Note that the jump around  $\simeq 3 \times 10^{-10}$  G and  $\simeq 2 \times 10^{-11}$  G, respectively, is due to the transition from ICS to synchrotron emission (at large fields) as dominant energy loss.

which, from Fig. 2, requires that synchrotron emission dominates the losses of the deflected pairs. In this case, a significant fraction of the energy flux going into pairs is deflected more than  $\sim (10/A) \times 6^\circ$ , thus modifying the  $\gamma$ -ray point flux at energies

$$E_\gamma \lesssim 2.2 \times 10^8 \text{ eV} \left( \frac{E_c(B, A)}{\text{EeV}} \right)^2 \left( \frac{B}{\text{nG}} \right). \quad (8)$$

In the following we will confirm these expectations with numerical simulations.

Within CRPropa, the parameter  $A$  can be chosen by the user, and the local contribution of electrons with energy  $E_e < E_c(B, A)$  to the  $\gamma$ -ray flux can be switched on or off: This allows to estimate the uncertainty in the  $\gamma$ -ray flux arriving within a certain angle  $\sim (10/A) \times 6^\circ$  from a point source due to the 1D approximation. An example is shown in Fig. 3, where the computed  $\gamma$ -ray fluxes from a single proton source located at 100 Mpc from the Earth in a uniform magnetic field of amplitude 100 pG are compared with and without cutting the charged component of the EM cascade deflected by more than  $6^\circ$  and  $0.6^\circ$ , respectively.

For the flux arriving within  $6^\circ$  in Fig. 3,  $E_c \simeq 3 \times 10^{14}$  eV, see Fig. 2, and

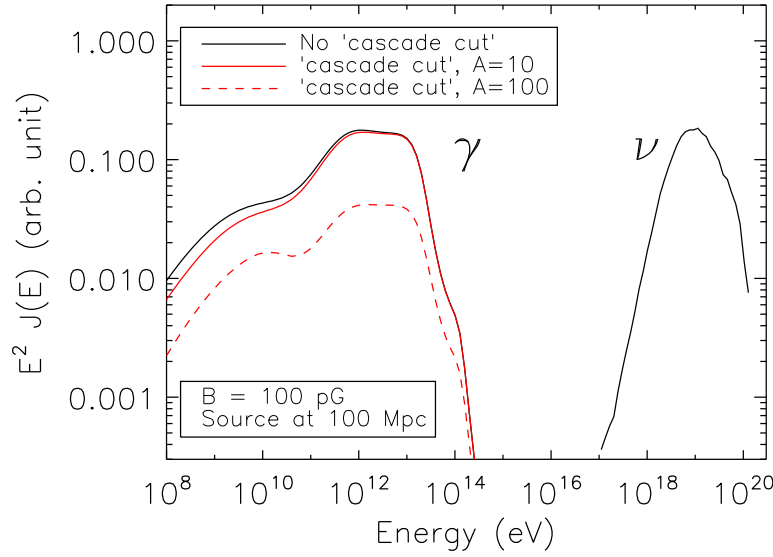


Fig. 3. Flux of secondary neutrinos (all flavors are added) and  $\gamma$ -rays from a single source of UHE protons with injection spectrum  $\propto E^{-2}$  up to  $5 \times 10^{20}$  eV, computed assuming a straight line propagation for the protons but taking into account the influence of a 100 pG magnetic field on the EM cascades. The red line is the flux computed by “cutting” the local  $e^{+/-}$  flux below  $E_c(B, A)$  (see text), for  $A = 10$  (continuous line) and  $A = 100$  (dashed line). This corresponds to pair deflections of  $6^\circ$  or  $0.6^\circ$ , respectively.

indeed a discernible but still modest,  $\sim 30\%$ , modification appears only for  $E_\gamma \lesssim 0.1$  TeV, where the photon energy flux becomes comparable to the pair energy flux around  $E_c$ .

For the flux arriving within  $0.6^\circ$  in Fig. 3,  $E_c \simeq 2 \times 10^{19}$  eV, see Fig. 2, and by the above argument and Eq. (8) we expect the photon flux to be significantly modified below  $\sim 10$  TeV. Indeed, at these energies the flux is reduced by a factor  $\sim 5$ .

In case of comparatively strong magnetic fields of order  $\mu\text{G}$ , typical in galaxy clusters,  $E_c \lesssim 10^{18}$  eV, and  $\gamma$ -ray point fluxes arriving within  $\sim 0.6^\circ$  should only be modified significantly for  $E_\gamma \lesssim 100$  GeV. Also note that for the production of secondaries inside a magnetized region where the parent UHECR particles are isotropically distributed, the full three dimensional treatment of the EM cascade is not necessary because for any  $e^-$  that is deflected away from the line of sight there is always another  $e^-$  that is deflected into the line of sight. In realistic situations, the magnetic fields are highly structured with typical amplitudes of  $\sim \mu\text{G}$  in the clusters, and  $\lesssim 10$  pG in the voids. The above discussion shows that in all these cases CRPropa can estimate the minimal  $\gamma$ -ray flux arriving within an angle  $(10/A) \times 6^\circ$  from the source.



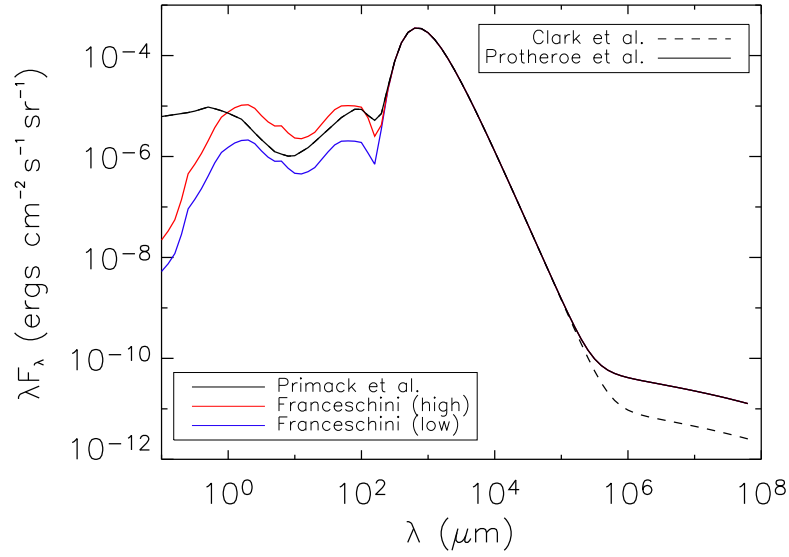


Fig. 4. Models implemented for the low energy photon background at zero redshift. The IRB consists basically of a peak in the far infrared around  $100\mu\text{m}$  dominated by dust and a peak in the near infrared dominated by stars.

### 2.3 Background Photon Spectra and their Evolution

Fig. 4 shows the EBL energy distributions that have been implemented. The most important is the CMB. For the infrared background (IRB) we implemented three distributions, a low and a high version of Franceschini et al. [14] which differ roughly by a factor 5, as well as the one by Primack et al. [15]. The low Franceschini et al. and the Primack et al. backgrounds are consistent with recent upper limits from blazar observations in TeV  $\gamma$ -rays by HESS [16]. For a recent review of the IRB see for example Ref. [17].

The IRB has a significant influence on EM cascades only around the threshold for pair production, i.e. between a few TeV and  $\simeq 100$  TeV. At higher energies, the  $\gamma$ -ray flux is suppressed by interactions with the CMB and, above  $\simeq 10^{19}$  eV, by interactions with the radio background. At energies below  $\sim$  TeV, the Universe acts as a calorimeter and the total photon flux is proportional to the total EM energy injected above  $\sim$  PeV with a rather universal shape [18].

Although its photon number density  $\simeq 2\text{ cm}^{-3}$  is a factor  $\simeq 200$  smaller than for the CMB, below the GZK-cutoff and above  $\sim 10^{17}$  eV the IRB can significantly reduce the nucleon mean free path for pion production. This can be important for secondary photon and neutrino [19,20] production, especially for a steep primary injection spectrum and/or strong redshift evolution.

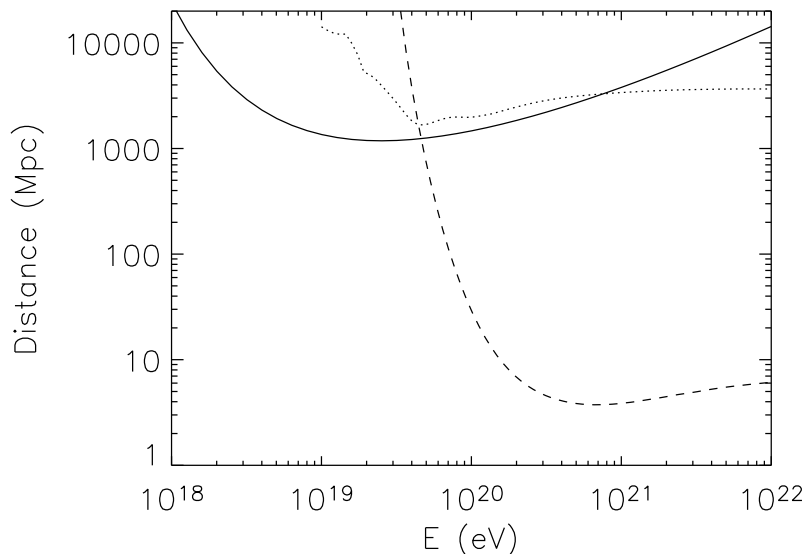


Fig. 5. Proton energy loss length for pair production on the CMB (continuous line), interaction length for pion production on the CMB (dashed line) and on the Primack et al. IRB (dotted line) at  $z = 0$ . The irregularities in the dashed curve are due to the piecewise power law fits of the Primack et al. IRB.

For the universal radio background (URB) we use a weak and a strong version based on Ref. [21] and on observations [22]. The URB is mostly important for EM cascades above  $\sim 10^{18}$  eV where it can inhibit cascade development due to the resulting small pair production lengths, especially for fast synchrotron losses of electrons in the presence of strong magnetic fields.

Since URB photons can give rise to pion production only above a few times  $10^{22}$  eV, where the interaction rate is essentially proportional to the total EBL photon density which is dominated by the CMB by a factor  $\sim 10^3$ , see Fig. 4, the URB is negligible for pion production. The same applies to pair production by protons.

Figs. 5 and 6 show interaction and energy loss lengths for protons and interaction lengths of photons, respectively, and their dependence on EBL models at zero redshift. This demonstrates that the IRB becomes important for pion production by protons below the GZK cutoff and for pair production by photons below the threshold in the CMB at  $\sim 10^{14}$  eV. It also shows that the URB tends to dominate pair production by photons above  $\sim 10^{19}$  eV.

The redshift evolution of the cosmic microwave background (CMB) is trivial. The redshift evolution of the radio and infrared distributions is more complicated: Ultra-relativistic particles of energy  $E$  injected at redshift  $z'$  with a rate per energy and comoving volume  $\Phi(E, z')$  result in a *physical* number density per energy at redshift  $z$  given by

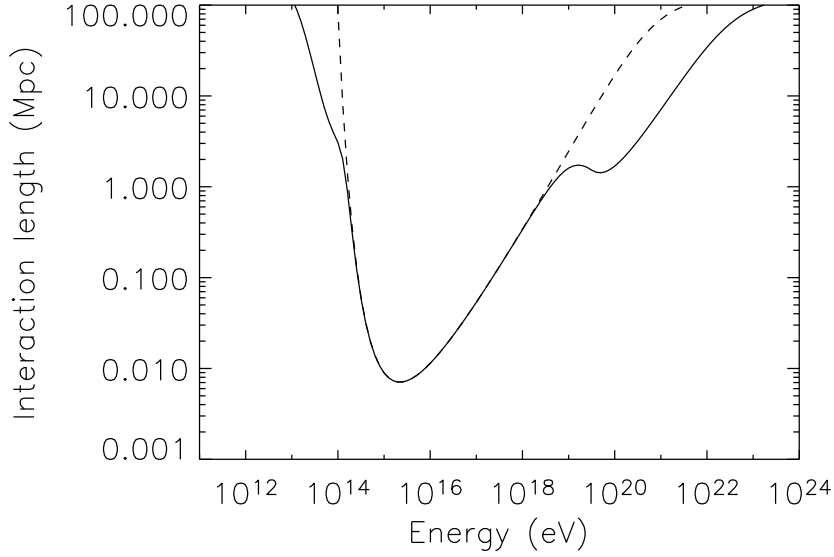


Fig. 6. Photon interaction length at  $z = 0$  on the EBL consisting of the CMB, the Primack et al. IRB, and the strong URB version. Dotted line: Interaction length in the CMB only at  $z = 0$ .

$$n(E, z) = (1+z)^3 \int_z^\infty dz' \frac{4\pi\Phi[E_i(E, z, z'), z']}{(1+z')H(z')} \times \frac{dE_i}{dE}(E, z, z'), \quad (9)$$

where it is assumed that the particle loses energy continuously such that its injection energy can be computed analytically,  $E_i(E, z, z')$ . Interactions of the low energy EBL photons, whose differential number densities we will denote by  $n_b(\varepsilon, z)$  in the following to distinguish from the high energy particles, can safely be neglected after recombination,  $z \lesssim 10^3$ , such that  $E_i(E, z, z') = (1+z')E/(1+z)$ . Eq. (9) then simplifies to

$$n_b(\varepsilon, z) = (1+z)^2 \int_z^\infty dz' \frac{4\pi\Phi[(1+z')\varepsilon/(1+z), z']}{H(z')}, \quad (10)$$

By using  $|dt/dz| = [(1+z)H(z)]^{-1}$ , one can see easily that the total energy density per comoving volume redshifts as  $\int d\varepsilon \varepsilon n_b(\varepsilon, z)/(1+z)^3 = (1+z) \int dt d\varepsilon_i \Phi(\varepsilon_i, z')/(1+z')$ , as it should be.

For the URB we implemented a nontrivial redshift evolution in the cascade module, as this can be relevant for EM cascade development. We assume that  $\Phi_{\text{URB}}(\varepsilon, z) = \phi_{\text{URB}}(\varepsilon)g_{\text{URB}}(z)$  factorizes into an energy dependence  $\phi_{\text{URB}}(\varepsilon)$  motivated by the observations [22] and theoretical estimates [21] and a redshift dependence given by

$$g_{\text{URB}}(z) = 10^{1.18z - 0.28z^2}, \quad (11)$$

as in Ref. [6].

For the Primack et al. IRB [15] we use for simplicity the differential photon energy distribution evolution

$$n_b(\varepsilon, z) = \begin{cases} (1+z)^2 n_b\left(\frac{\varepsilon}{1+z}, z=0\right) & \text{for } z \leq z_b, \\ 0 & \text{otherwise} \end{cases} \quad (12)$$

which corresponds to instantaneous creation of the background at redshift  $z_b$  with  $\Phi(\varepsilon, z') = H(z_b) n_b[\varepsilon/(1+z_b), z=0] \delta(z' - z_b)/(4\pi)$  in Eq. (10). It strictly applies to the CMB which was effectively produced at decoupling,  $z_b \sim 1100$ . For the IRB we assume  $z_b = 5$ . Interaction lengths  $l(E, z)$  and, in case of continuous energy loss processes such as PPP, energy loss rates  $b(E, z) \equiv dE/dt$  then follow simple scaling relations in redshift [20],

$$\begin{aligned} l(E, z)^{-1} &= (1+z)^3 l[(1+z)E, z=0]^{-1} \\ b(E, z) &= (1+z)^2 b[(1+z)E, z=0]. \end{aligned} \quad (13)$$

This simplifies implementation in SOPHIA.

#### 2.4 Distributions and Properties of Sources

Both single sources and realizations of both discrete or continuous source distributions can be used in CRPropa. In the latter case, the distributions can be selected, for example, to follow the baryon density from a large scale structure simulation box, and are periodically repeated.

The UHECR particles are injected isotropically around the sources with a monochromatic or a power-law energy distribution between a minimal and a maximal energy,  $E_{\min}$  and  $E_{\max}$ , respectively:

$$\frac{dN}{dE_{\text{inj}}} \propto E_{\text{inj}}^{-\alpha} \quad E_{\min} \leq E_{\text{inj}} \leq E_{\max}$$

For each trajectory reaching the observer and being registered, the source identity  $i$  is also registered. This allows to apply a re-weighting procedure on the recorded “events”, in order to vary individual source properties such as their injection power law index  $\alpha_i$  or luminosity  $Q_i$ . For example, it is most efficient in terms of CPU time to inject the UHECRs with a spectral index  $\alpha_0 = 1$  at the sources, that is with a uniform distribution in the logarithm of the energy. By re-weighting each recorded event by a factor  $w \propto Q_i E_{\text{inj}}^{\alpha_i - 1}$ , the

source  $i$  would contribute with a power  $Q_i$  and an effective injection power law index  $\alpha_i$  in all observables constructed from the weighted trajectory sample.

### 3 Large Scale Structure and Magnetic Fields

The strength and distribution of the EGMF is currently poorly known and their impact on UHECR are hard to quantify, as demonstrated by the different results in Refs. [5,23]. See also Ref. [24] for a discussion of these differences and Ref. [25] for a review on EGMF. We note that there are recent observational hints of EGMF as strong as  $\sim 0.1 \mu\text{G}$  on scales as extended as superclusters [26], as well as theoretical motivations for such fields [27].

Enhanced magnetic fields around large scale structures such as galaxy clusters together with associated larger EBL densities can lead to increased production of  $\gamma$ -rays and neutrinos.

The EGMF from the large scale structure simulation from Ref. [28,29] has so far been implemented in CRPropa, but any magnetic field model can be used. Within the public package CRPropa, only a small subgrid of the simulations from [28,29] is provided in order to allow simple tests. Fig. 7 shows a 2D cross section through the environment of a galaxy cluster from this simulation. In this simulation, the magnetic fields follow the baryon density, and in particular the regions that are filled with sub- $\mu\text{G}$  fields are quite extended around the large-scale structures (with a typical extension of a few Mpc). This is due, in particular, to the fact that magnetic fields are generated at the LSS shocks within that model. Of course, the properties of  $\gamma$ -ray sources associated with UHECR sources as well as the feasibility of “charged particle astronomy” depend strongly on the magnetic field model [24], [23].

Large scale structure simulations usually cover only a small fraction of today’s Universe, typically of order 100 Mpc in linear scale. Since sources at much larger, cosmological distances can contribute to the fluxes of UHECR below the GZK cutoff, of photons below  $\sim \text{TeV}$  and of neutrinos, the EGMF and source distributions are periodically continued in the 3D version of the code. EGMF with homogeneous statistical properties and power law spectra in Fourier space (e.g a Kolmogorov spectrum) have also been implemented in the package.

### 4 Simple Applications

We present here applications of CRPropa that are obtained with very simple configurations requiring little CPU time. The results can easily be compared

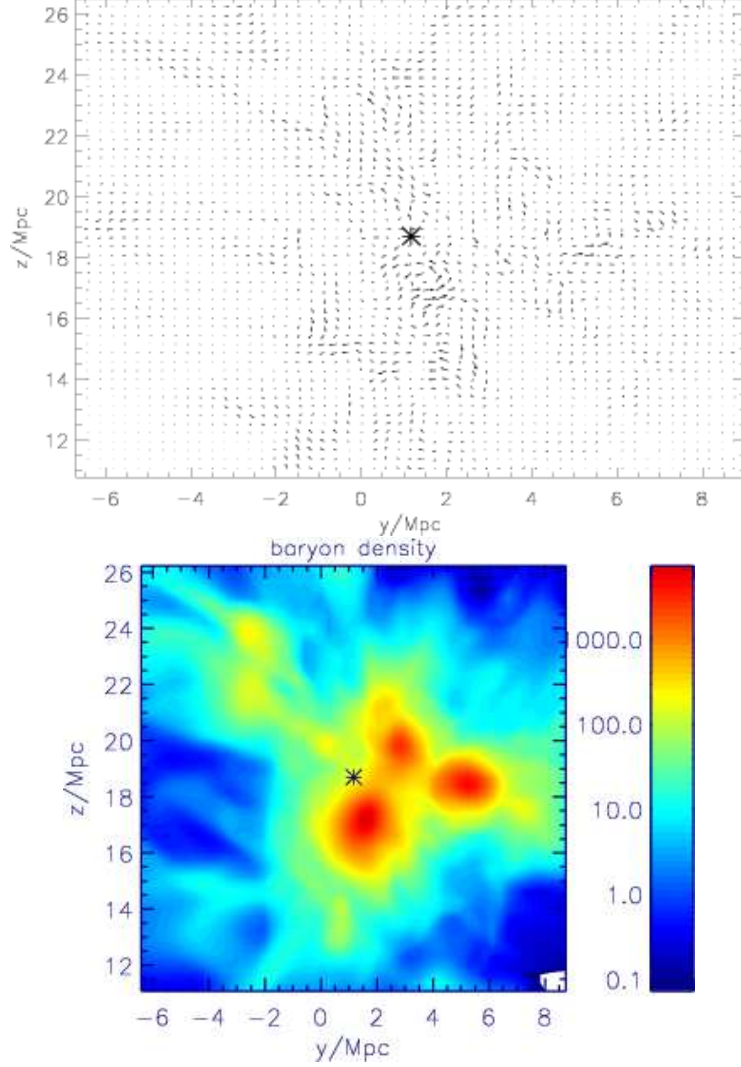


Fig. 7. A 2D cross section through the relative size and polarization of the EGMF in linear scaling, (top panel) and the relative baryon density in logarithmic scaling (bottom panel) in the environment of a galaxy cluster from the simulations from Ref. [28,29].

with previous results from the literature.

Fig. 8 shows the averages and dispersions of the energy of nucleons in a one-dimensional simulation, as a function of propagated distance for various initial energies. Using SOPHIA automatically enables us to reproduce the stochasticity of pion production.

Fig. 9 shows the spectra of secondaries generated during the one-dimensional propagation of UHECRs from a source located at 20 Mpc or 100 Mpc from the observer. Note that the neutrino flux increases with distance to the source, whereas the photon flux above  $\sim 10^{14}$  eV decreases, but the photon flux below this energy increases. This is because more secondary neutrinos and EM par-

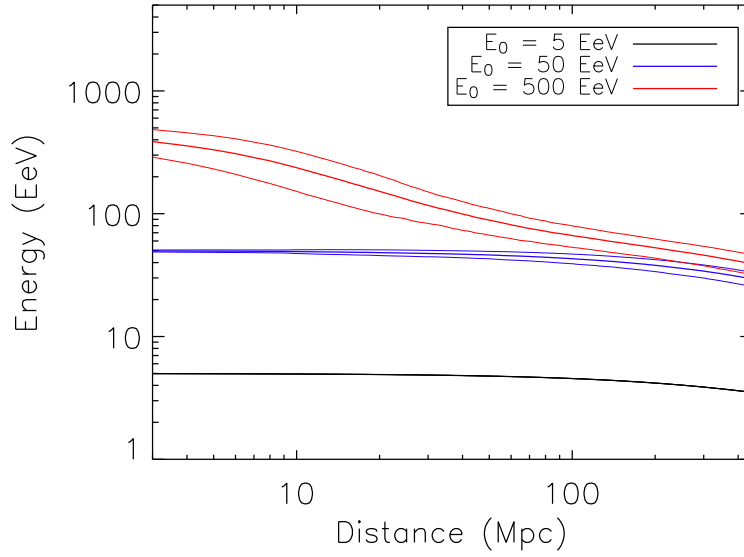


Fig. 8. Evolution of the energy of nucleons as a function of propagation distance, for initial energies of 5, 50 or 500 EeV. The thin lines indicate the dispersion induced by the stochasticity of pion production.

ticles are produced for larger propagation distances, but EM particles above  $\sim 10^{14}$  eV are quickly degraded and cascade down to sub-PeV energies. A more detailed analysis of the fluxes of secondaries from a single UHECR source (e.g. the relative contribution of pair production and pion production on the  $\gamma$ -ray flux) can be found in Ref. [13]. The study of secondary photons from UHECR sources has also been carried out in various situations in Refs [30,31,32,33,34].

Fig. 10 shows the spectra of secondary neutrinos from a source located at 20 Mpc from an observer, depending in particular on the magnetic field effects. It is remarkable that, for a given source luminosity, the flux of secondary neutrinos is increased by a factor of more than two due to the enhancement of the UHECR propagation distance generated by the  $\mu$ G-level magnetic fields that surround this source.

Fig. 11 compares the spectral shape of UHECRs from a source located at 100 Mpc from an observer, depending on the presence of magnetic fields around the source. If magnetic fields of amplitude  $\sim \mu$ G surround the source over a few Mpc, the observed spectrum is clearly modified: 1) there is a dispersion in the true propagation distance, compared to a fixed propagation distance of 100 Mpc. This reduces the amplitude of the "bump"; 2) the mean propagation distance is increased compared to 100 Mpc. This leads to a GZK cut-off at slightly lower energies.

Fig. 12 compares the spectra obtained with CRPropa to the one presented on the red curve of Fig.14 in [35] for a model of cosmologically distributed

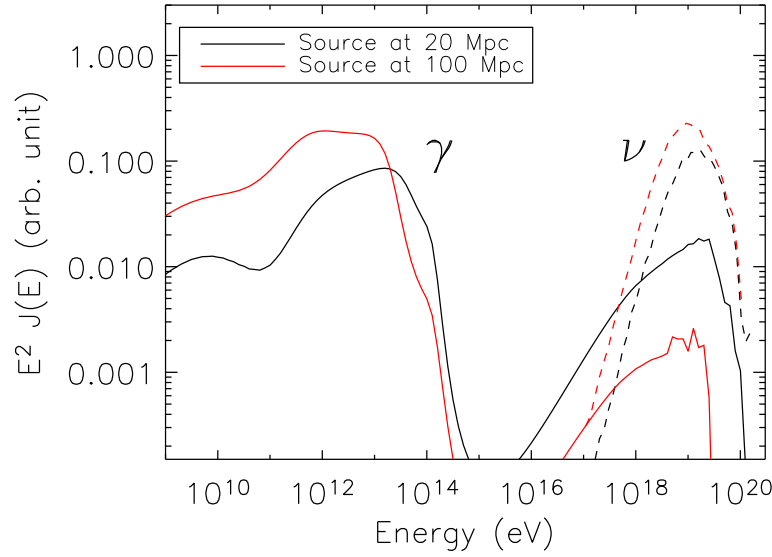


Fig. 9. Spectrum of secondary photons and neutrinos (all flavors added) generated by pion and pair production from a single UHECR source at a given distance. We consider here a one-dimensionnal model, with an injection spectral index  $\alpha = 2$  for the UHECRs. A uniform magnetic field of 0.1 nG is assumed. Note that below  $\sim$ TeV the  $\gamma$ -ray flux would be spread over several degrees and that, as shown in Fig. 3, the 1D approximation of the EM cascade does not significantly affect the accuracy of the  $\gamma$ -ray flux arriving within such angles. The fluctuations at the highest energies are statistical.

proton sources with spectral index  $\gamma_s = 2.6$  and a source evolution parameter  $m = 2.4$ . We see that, for a given model, the spectrum estimations obtained with our Monte-Carlo method and with a direct integration of the transport equations (for [35]) agree within a few %. The blue and red curves of the lower panel in Fig. 12 show the influence of two numerical parameters on the accuracy of the derived spectrum at the highest energies. The maximum injection energy allowed in the Monte-Carlo has an influence at energies above  $10^{20}$  eV, in agreement with results shown, for example, in Fig.5 of [35]. The use of a propagation stepsize of 0.3 Mpc instead of 1 Mpc does not lead to a significant change in the simulated spectrum. Other tests showed that using a propagation stepsize of 5 Mpc instead of 1Mpc results in a  $\sim 10\%$  overestimation of the spectrum in the specific energy range  $100 < E < 160$  EeV, and an underestimation of the spectrum at higher energies. A 1 Mpc stepsize is therefore reasonable to reach the typical accuracies required for comparison with current and forthcoming experimental data.



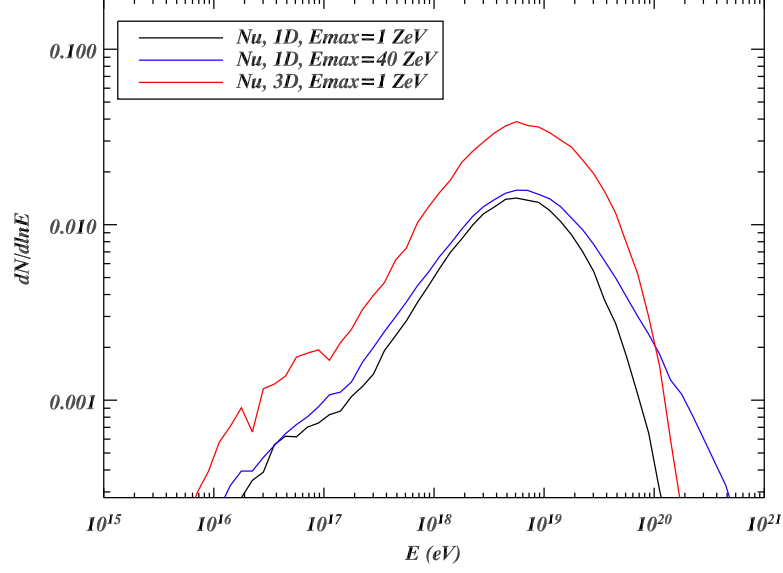


Fig. 10. Secondary neutrinos (all flavors added) from a nearby source of UHECRs with a given luminosity. The flux increases at high energies both with maximum UHECR acceleration energy and with the strength of magnetic fields surrounding the source. The fluctuations at low energy are statistical. The  $y$ -axis is in arbitrary units.

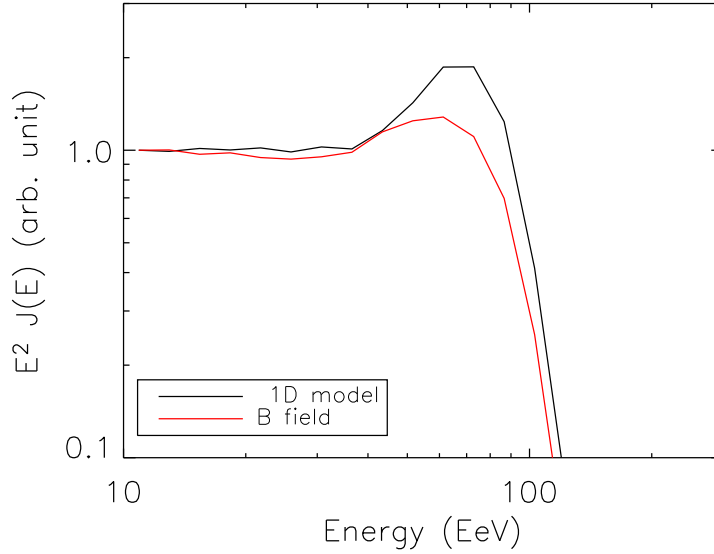


Fig. 11. UHECR spectrum from a source located at 100 Mpc from an observer, injecting protons with a spectrum  $\propto E^{-2}$  up to  $E_{\text{max}} = 10^{21}$  eV. The red curve is obtained from a full 3-dimensional simulation, where the source is embedded in a region with  $\mu\text{G}$  fields over a few Mpc.

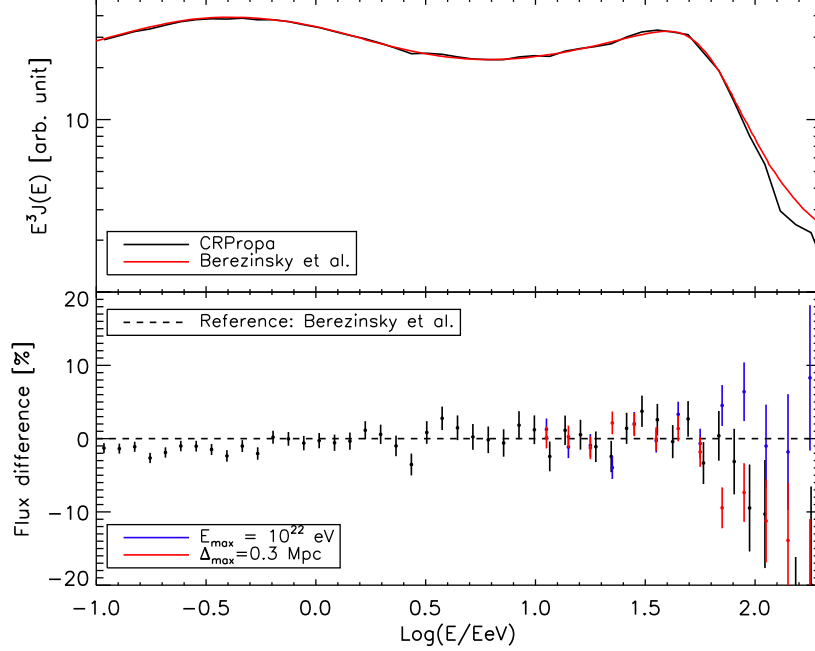


Fig. 12. Top: Comparison of the spectra obtained with CRPropa to the one found in [35] for a model of cosmologically distributed sources. The specific parameters of the model correspond to the red curve of Fig.14 in [35]. We use a propagation stepsize of 1Mpc and a maximum injection energy of  $10^{21}$  eV. Bottom: Relative difference with respect to the curve of [35](black). The error bars are the statistical uncertainties due to the finite number of propagated nucleons. Red: same, for a simulation using a stepsize of 0.3 Mpc. Blue: same, for a simulation using a maximal injection energy of  $10^{22}$  eV.

## 5 Conclusions

We have presented the first public package to study systematically the properties of the propagation of UHECRs and their secondaries in a structured magnetized Universe. We have detailed the interactions that are already implemented, and presented a few simple examples obtained directly by running the CRPropa code.

A major advantage of CRPropa is its large modularity, which should allow various users to implement their own modules, adapted to specific UHECR propagation models. Many possible upgrades of the CRPropa package can be considered: This includes the implementation of non-uniform grids for magnetic field models, of UHE nuclei and secondary neutrinos and EM particles from their interactions, of inhomogeneous low energy target photon backgrounds for the UHE nuclei and EM cascade interactions, and of hadronic interactions with the baryon gas in dense parts of the large scale structure. Finally, interactions of UHE neutrinos with relic neutrinos of arbitrary mass and clustering properties could also be implemented, including the resulting

secondary particles.

## Acknowledgements

FM acknowledges partial support by the Swiss Institute of Technology through a Zwicky Prize Fellowship. We thank all the people who built the previous codes from which the development of CRPropa has largely taken profit, in particular Martin Lemoine, Gianfranco Bertone, Claudia Isola, and Sangiin Lee. We also thank Sébastien Renaux-Pétel for useful tests.

CRPropa makes use of the public code SOPHIA [7], and the TinyXML [36], CFITSIO [37] and CLHEP [38] libraries.

## References

## References

- [1] J. W. Cronin, Nucl. Phys. B (Proc. Suppl.) **28B** (1992) 213; The Pierre Auger Observatory Design Report (ed. 2), March 1997; see also <http://www.auger.org>.
- [2] for recent reviews see, e.g., F. Halzen and D. Hooper, Rept. Prog. Phys. **65**, 1025 (2002) A. B. McDonald, C. Spiering, S. Schonert, E. T. Kearns and T. Kajita, Rev. Sci. Instrum. **75**, 293 (2004)
- [3] for recent short reviews see, e.g., H. J. Völk, [astro-ph/0401122](#); H. J. Völk, [astro-ph/0312585](#).
- [4] K. Greisen, Phys. Rev. Lett. **16**, 748 (1966); G. T. Zatsepin and V. A. Kuzmin, JETP Lett. **4**, 78 (1966) [Pisma Zh. Eksp. Teor. Fiz. **4**, 114 (1966)].
- [5] G. Sigl, F. Miniati and T. A. Ensslin, Phys. Rev. D **70**, 043007 (2004) [astro-ph/0401084](#).
- [6] S. Lee, Phys. Rev. D **58**, 043004 (1998) [astro-ph/9604098](#).
- [7] A. Mücke, R. Engel, J. P. Rachen, R. J. Protheroe and T. Stanev, Comput. Phys. Commun. **124**, 290 (2000)
- [8] G. R. Blumenthal, Phys. Rev. D **1**, 1596 (1970).
- [9] M. J. Chodorowski, A. .A. Zdziarski, M. Sikora, Astrophys. J. **400**, 181 (1992).
- [10] A. Mastichiadis, Mon. Not. Roy. Astron. Soc. **253**, 235 (1991).
- [11] A. Mastichiadis, R. J. Protheroe and J. G. Kirk, Astron. Astrophys. **433**, 765 (2005) [astro-ph/0501156](#).

- [12] P. Bhattacharjee and G. Sigl, Phys. Rept. **327**, 109 (2000) [astro-ph/9811011](#).
- [13] E. Armengaud, G. Sigl and F. Miniati, Phys. Rev. D **73**, 083008 (2006) [astro-ph/0511277](#).
- [14] A. Franceschini, H. Aussel, C. J. Cesarsky, D. Elbaz and D. Fadda, Astron. Astrophys. **378**, 1 (2001).
- [15] see, e.g., J. R. Primack, J. S. Bullock and R. S. Somerville, AIP Conf. Proc. **745**, 23 (2005) [astro-ph/0502177](#).
- [16] F. Aharonian *et al.* [H.E.S.S. Collaboration], [astro-ph/0508073](#).
- [17] G. Lagache, J. L. Puget and H. Dole, [astro-ph/0507298](#).
- [18] P. S. Coppi and F. A. Aharonian, Astrophys. J. **487**, L9 (1997) [astro-ph/9610176](#).
- [19] T. Stanev, Phys. Lett. B **595**, 50 (2004) [astro-ph/0404535](#).
- [20] E. V. Bugaev, A. Misaki and K. Mitsui, Astropart. Phys. **24**, 345 (2005) [astro-ph/0405109](#).
- [21] R. J. Protheroe and P. L. Biermann, Astropart. Phys. **6**, 45 (1996) [Erratum-*ibid.* **7**, 181 (1997)] [astro-ph/9605119](#).
- [22] T. A. Clark, L. W. Brown and J. K. Alexander, Nature **228**, 847 (1970).
- [23] K. Dolag, D. Grasso, V. Springel and I. Tkachev, JETP Lett. **79**, 583 (2004) [Pisma Zh. Eksp. Teor. Fiz. **79**, 719 (2004)] [astro-ph/0310902](#); K. Dolag, D. Grasso, V. Springel and I. Tkachev, JCAP **0501**, 009 (2005) [astro-ph/0410419](#).
- [24] G. Sigl, F. Miniati and T. Ensslin, Nucl. Phys. Proc. Suppl. **136**, 224 (2004) [astro-ph/0409098](#).
- [25] P. P. Kronberg, Reports of Progress in Physics 58 (1994) 325; J. P. Vallée, Fundamentals of Cosmic Physics, Vol. 19 (1997) 1; T. E. Clarke, P. P. Kronberg, and H. Böhringer, Astrophys. J. Lett. 547 (2001) L111; J.-L. Han and R. Wiełebinski, Chinese Journal of Astronomy and Astrophysics 2 (2002) 293 [astro-ph/0209090](#); P. P. Kronberg, Physics Today 55, December 2002, p. 40.
- [26] Y. Xu, P. P. Kronberg, S. Habib and Q. W. Dufton, [astro-ph/0509826](#).
- [27] M. V. Medvedev, L. O. Silva and M. Kamionkowski, [astro-ph/0512079](#).
- [28] D. Ryu, H. Kang, and P. L. Biermann, Astron. Astrophys. **335** (1998) 19.
- [29] F. Miniati, Mon. Not. Roy. Astron. Soc. **337**, 199 (2002) [astro-ph/0203014](#).
- [30] S. Gabici and F. A. Aharonian, [astro-ph/0505462](#).
- [31] C. Ferrigno, P. Blasi and D. De Marco, Astropart. Phys. **23**, 211 (2005)

- [32] C. Rordorf, D. Grasso and K. Dolag, *Astropart. Phys.* **22**, 167 (2004)
- [33] S. Inoue, F. A. Aharonian and N. Sugiyama, *Astrophys. J.* **628**, L9 (2005)
- [34] F. A. Aharonian, *Mon. Not. Roy. Astron. Soc.* **332**, 215 (2002).
- [35] V. Berezhinsky, A. Z. Gazizov and S. I. Grigorieva, *Phys. Rev. D* **74**, 043005 (2006) [hep-ph/0204357](#).
- [36] <http://www.grinninglizard.com/tinyxml/>
- [37] <http://heasarc.gsfc.nasa.gov/docs/software/fitsio>
- [38] <http://www.cern.ch/clhep/>